Spin-wave excitation in the antiferromagnetic bilayer ruthenate Ca_{3}Ru_{2}O_{7}

X. Ke, Tao Hong, J. Peng, S. E. Nagler, G. E. Granroth, M. D. Lumsden, and Z. Q. Mao

Phys. Rev. B **84**, 014422 — Published 27 July 2011

DOI: 10.1103/PhysRevB.84.014422

Spin wave excitation in the antiferromagnetic bilayer ruthenate $Ca_3Ru_2O_7$

X. Ke[1], Tao Hong[1], J. Peng[2], S. E. Nagler[1], G. E. Granroth[1], M. D. Lumsden[1], and Z. Q. Mao[2]

[1]*Neutron Scattering Science Division, Oak Ridge National Laboratory, Oak Ridge, TN 37831, USA*

[2]*Department of Physics and Engineering Physics, Tulane University, New Orleans, Louisiana 70118, USA*

We study the spin wave excitation spectrum of the antiferromagnetic bilayer ruthenate $Ca_3Ru_2O_7$ through inelastic neutron scattering measurements. The material behaves as a quasi-two dimensional ferromagnetic bilayer system with very weak interbilayer antiferromagnetic coupling and its magnetic dispersion can be well described with a nearest-neighbor Heisenberg model. We find that the intrabilayer exchange interaction along the out-of-plane c-axis is much stronger than the in-plane intralayer interaction, in sharp contrast to the previously reported bilayer manganite system. And our study reveals a finite lifetime effect of the magnetic excitation, presumably attributable to existence of a small number of itinerant charge carriers within the planes.

There has been intensive research in the Ruddlesden-Popper type ruthenates $(Sr_{1-x}Ca_x)_{n+1}Ru_nO_{3n+1}$ in the past decade, largely stimulated by the observation of various exotic physical phenomena in these materials, which sensitively depend on the value of Ca doping concentration x and the layer number n [1]. Compared with the unconventional superconductivity observed in the single layer (n = 1) compound Sr_2RuO_4 [2] and the itinerant ferromagnetism in $SrRuO_3$ with infinite layers (n = ∞) [3], the bilayer strontium ruthenate $Sr_3Ru_2O_7$ exhibits paramagnetic Fermi liquid feature at zero magnetic field [4], and behaves as a metamagnetic quantum critical system with a nematic electron liquid phase at high fields [5,6]. Inelastic neutron scattering measurements reveal incommensurate magnetic fluctuations in both Sr_2RuO_4 [7,8,9] and $Sr_3Ru_2O_7$ [10,11], which are attributed to strong Fermi surface nesting.

Substitution of Ca for Sr sites introduces additional rotation/tilt of RuO_6 octahedra due to the smaller ion radius of Ca^{2+}. This difference significantly alters the structural, magnetic, and electronic properties of the Ca-based ruthenates. For instance, the ground state of $Sr_{2-x}Ca_xRuO_4$ evolves from superconductor (x = 0) to antiferromagnetic Mott insulator (x = 1), accompanied with the structure transition and enhanced magnetic fluctuations for intermediate x [12,13,14]. Likewise, the physical properties of $Sr_{3-x}Ca_xRu_2O_7$ sensitively depend on the Ca concentration [4,15,16,17,18,19,20]. For the end members, $Ca_3Ru_2O_7$ undergoes an antiferromagnetic ordering transition at T_N ~ 56 K followed by a first-order metal-insulator transition at T_{MI} ~ 48 K [19], which is dramatically distinct from the paramagnetic behavior observed in $Sr_3Ru_2O_7$ [4]. Recent neutron diffraction measurements [21,22] on $Ca_3Ru_2O_7$ show a commensurate magnetic structure with the magnetic moment ferromagnetically aligned within the RuO_2 bilayers and antiferromagnetically aligned between the bilayers, as shown in Fig. 1. This ordered structure successfully explains the giant magnetoresistance behavior within the spin-valve framework

[19,22,23,24]. Despite the intriguing magnetic structure and the exotic electronic properties of $Ca_3Ru_2O_7$, little is known about its spin dynamics. Raman scattering has been used to probe the magnetic excitations at the zone center [20,25], but the magnetic dispersion relation of this material was unknown until this present study. Such information is essential to characterize the strength of the magnetic exchange interactions and thus better understand the magnetic behavior of this system.

In this work we present the first study on spin wave excitations in $Ca_3Ru_2O_7$ single crystals by inelastic neutron scattering. Our results confirm the quasi-two dimensional character of the system, and can be described in the framework of the Heisenberg model. We find that the intrabilayer ferromagnetic interaction along the *c*-axis ($J_\perp$) is much stronger than the in-plane intralayer interaction ($J_{//}$), in contrast to the bilayer manganite system which possesses a bilayer magnetic structure similar to that of $Ca_3Ru_2O_7$ but exhibits magnetic interactions with $J_{//}/J_\perp \geq 1$ [26,27,28]. Furthermore, our study reveals a measurable, albeit small, finite lifetime of the magnetic excitations, which can possibly be attributed to the existence of itinerant charge carriers within the planes.

Single-phase $Ca_3Ru_2O_7$ single crystals were grown using the floating-zone technique in a mirror-focused furnace. Three single crystals, with a total mass of ~ 3 grams, were co-aligned with the FWHM ~ 1.5 degree. Inelastic neutron scattering experiments were performed using HB1 and HB3 thermal neutron triple-axis spectrometers at High Flux Isotope Reactor (HFIR) in Oak Ridge National Laboratory. The neutron final energy E_f was fixed as 14.7 meV except where otherwise specified and collimations was set to be 48'-40'-40'-70'. Orthorhombic crystal structure indices of the material were used with a_0 = 5.366 Å, b_0 = 5.522 Å, and c_0 = 19.49 Å.

Samples were cooled down in a top-loading displex with the (H 0 L) scattering plane aligned, where H and L are the reciprocal lattice indices. Based on crystal symmetry and the magnetic structure shown in Fig. 1, nuclear Bragg diffraction requires H and L be even or the sum of H and L be even, while magnetic Bragg diffraction peaks appears at (H 0 L) with even H and odd L values [22]. All data presented here were measured at T = 10 K unless specifically noted. Neutron intensity is presented in the unit of counts / MCU, where MCU represents the monitor count unit with 1 MCU corresponding to a counting time of approximately 1 minute.

Figure 2(a) shows energy scans at $\boldsymbol{Q}$ = (0 0 5), (0 0 4.5) and (0 0 6). There are two main features one can clearly see from the figure. One is that the peak in intensity occurs at $E \sim 7$ meV at the magnetic zone center $\boldsymbol{Q}$ = (0 0 5), indicating the magnetic excitation is gapped, with a value consistent with the one obtained from the Raman scattering measurements [20,25]. Such an energy gap arises from the magnetic anisotropy with the magnetic easy axis directed along the b-axis below T_{MI} as shown in Fig. 1 [22]. This is distinct from the very small energy gap reported in the bilayer manganite system [26,27,28]. Second, the magnetic excitation is essentially independent of L with the maximum intensity still near E = 7 meV, within the tolerance of instrumental energy resolution, even at the magnetic zone boundary $\boldsymbol{Q}$ = (0 0 6). This result reveals very weak interbilayer magnetic interactions as is expected due to the separation of RuO_2 bilayers by CaO planes. It is further confirmed by L-dependence of scattering intensity at the energy gap intensity as presented in Fig. 2(b). These data are well fit by $I \sim F^2(Q)\cos^2(\pi L\Delta / c_0)$ plus a constant background term, where $F(Q)$ is the Ru magnetic form factor and $\Delta \approx 0.1987 c_0$ is the intrabilayer separation (*i.e.*, the Ru-Ru distance in two adjacent layers along the c-axis). The described model is consistent with an in-phase fluctuation within the bilayer plane but little correlation between the bilayers. Such an L dependence of intensity is also

observed in $Sr_3Ru_2O_7$ [10,11], despite the dramatically different nature of the magnetic ground states as described above, and in the bilayer manganite system $La_{2-2x}Sr_{1+2x}Mn_2O_7$ with a similar bilayer magnetic structure [26,28]. These three cases suggest that such a Q dependence is a generic feature of magnetic bilayer systems. And it persists to high temperatures, even with T well above T_N, as illustrated by the data taken at 80 K shown in Fig. 2(b). This temperature dependence demonstrates the development of strong two-dimensional magnetic correlations prior to the onset of the magnetic long range order. These results, together with the strong magnetic dispersion along both H and K directions (to be discussed later), indicates that $Ca_3Ru_2O_7$ behaves as a quasi-two dimensional ferromagnetic system.

We now consider the H-dependence of the magnetic excitation. The inelastic intensity as a function of energy along (H 0 5) with various values of H is plotted in Fig. 3(a). Departing away from the zone center (0 0 5), the spectrum maximum shifts to higher energy with increasing H in the same Brillouin zone, characteristic of the magnetic dispersion along the (1 0 0) axis. A contour map of E-(H 0 5) plot with a step size $\Delta H = 0.05$ is given in Fig. 3(b), which clearly shows a feature of spin-wave like dispersion. Note that the spikes at higher H values are spurious scattering from accidental Bragg reflections.

In order to analyze the experimental results and extract the magnetic exchange interactions, we start with a Heisenberg model within a framework of localized magnetic moment on Ru sites. As discussed earlier, $Ca_3Ru_2O_7$ can be treated as a quasi-two dimensional system with a negligible interbilayer magnetic interaction. Therefore, the simplified magnetic Hamiltonian with the nearest-neighbor interactions is expressed as:

$$H = \frac{1}{2}\sum_{i,l}\vec{S}_{i,l} \bullet (J_{\perp}\vec{S}_{i,l+\Delta} + \sum_{\delta} J_{//}\vec{S}_{i+\delta,l}) + D\sum_{i,l}(S_{i,l}^{z})^2 \qquad (1)$$

where $J_\perp$ is the intrabilayer coupling along the c-axis, $J_{//}$ is the in-plane intralayer coupling as shown in the Fig. 1, and D is the spin anisotropy. Both $J_\perp$ and $J_{//}$ are negative, corresponding to ferromagnetic spin interaction within the bilayers (to be shown below). $\vec{S}_{i,l}$ represents the spin operator at the *i*th sites in the *l*th layer and Δ is the intrabilayer separation presented above. We then derive the expression for the magnetic dispersion after making the linear spin wave Holstein-Primakoff transformation and Bogoliubov transformation, which is written as:

$$\hbar\omega(q) = S(-J_{//}(z-\gamma_k) - J_\perp + D) \pm SJ_\perp \qquad (2)$$

Here $z = 4$ is the z-coordination of the Ru^{4+} ions, $\gamma_k = 4\cos(H\pi)\cos(K\pi)$, S is the magnitude of spin, and q is the reduced wave vector, the magnitude of which is equal to H in this study. The +(-) sign of the last term in Eq. 2 corresponds to the acoustic (optic) mode of the spin wave excitation associated with the two magnetic atoms in the primitive unit cell. Eq. 2 shows that the dispersion behavior of the optic mode is essentially similar to that of the acoustic mode by simply shifting the latter one by a value of $2SJ_\perp$. And the corresponding inelastic neutron scattering intensity is proportional to $\cos^2(\pi L\Delta/c_0)$ or $\sin^2(\pi L\Delta/c_0)$ for the acoustic or optic branch of the dispersion respectively, which maximizes at $L \sim 2.5n$ with n being even for the former branch and odd for the latter one. Therefore, the spin wave dispersion shown in Fig. 3(b) is associated with the acoustic (ac) mode, with $\hbar\omega_{ac}(q) = -4SJ_{//}(1-\cos(H\pi)) + SD$, which does not depend on $J_\perp$. The fit to the dispersion as illustrated by pink curve shown in Fig. 3(b) gives the spin gap energy *SD* of 7 meV as discussed above and the in-plane interlayer magnetic exchange interaction $SJ_{//} \sim -\frac{15}{4}$meV. Note that the magnetic dispersion along the K direction,

measured in the (0 *K L*) scattering plane (data not shown), is similar to the one observed along the *H* direction, as indicated by Eq. 2.

We attempt to obtain the intrabilayer interaction along the *c*-axis $J_{\perp}$. Specially, a constant-*Q* scan was measured at $\boldsymbol{Q}$ = (0 0 7.5), chosen to maximize the neutron scattering intensity of the optic branch of spin wave as described earlier and allowing for a large range of energy transfer while avoiding background associated with the direct neutron beam. No signal was observed above background that could be associated with the magnetic excitation for energy transfer as high as 20 meV. (Note that if there were maximum intensity at $E \sim 20$ meV, its value is estimated to be ~ 1/6 of the peak intensity at 7 meV measured at (0 0 5) when taking into account the effect of magnetic form factor and the decrease of neutron intensity with the increase of energy transfer, which should be still discernible from the background signal. With further increasing the energy transfer, the magnetic neutron scattering intensity continues to decrease while the background signal increases.) This suggests $|SJ_{\perp}| > \frac{13}{2}$ meV according to Eq. 2, and it is confirmed by another constant-*Q* measurement at $\boldsymbol{Q}$ = (0 0 3.75) with *E* ranging from 2 meV to 15 meV where only the 7 meV peak representing the energy gap associated with acoustic mode was observed. The large value of $J_{\perp}$ is consistent with results of density functional calculations where $J_{\perp}$ was calculated to be about 4 times of $J_{//}$ [24]. (That is, $|SJ_{\perp}|$ is expected to be about 37 meV. Note that the spectrum would be too broad at this energy to extract any meaningful intrinsic magnetic scattering intensity out of the background signal.) This is presumably associated with the stronger hybridization between Ru (d_{xy},d_{xz} and d_{yz}) orbitals in t_{2g} and the O p orbital owing to the relatively smaller Ru-O distance along the c-axis in the intrabilayer than the in-plane one. The stronger $J_{\perp}$ feature in $Ca_3Ru_2O_7$ is in stark contrast to

what has been observed in the bilayer manganite system $La_{2-2x}Sr_{1+2x}Mn_2O_7$ [26,27,28] with $J_{//}/J_{\perp} \geq 1$ that is argued to be due to the dominant $d_{x^2-y^2}$ planar orbital in the Mn e_g band which enhances the in-plane double-exchange ferromagnetic interaction [27,28].

Another intriguing feature in the magnetic excitation curves shown in Fig. 3(a) is the broadening of magnetic excitation with increasing *H*. The values of the peak width are larger than the single point instrumental energy resolution at larger *H* values which are calculated using Reslib program [29] and presented by the solid black lines in the figure. With the magnitude of *H* approaching 0.5 or higher values within the same Brillouin zone, the magnetic excitation curve is quite broad in addition to the significant decrease of the neutron scattering intensity, which makes the magnon signal hard to be resolved from the background signal. Such an increase in linewidth and decease in intensity of the magnon excitation spectra has been observed in rare-earth manganites (including both bilayer [28,30] and infinite layer systems [31,32]) around the zone boundary, which is argued to be due to either magnon-phonon interaction arising from the magnetic and lattice coupling [32], or due to the Stoner continuum resulting from the metallic ferromagnetic nature of the manganites [30,31] at low temperatures.

In an attempt to clarify the mechanisms of the broadening and decreasing in intensity of the magnetic excitation spectra observed in $Ca_3Ru_2O_7$, we have fit the convolution of $I \propto F^2(Q)S(q,\omega)\cos^2(\pi L\Delta/c_0)$ and the full instrumental resolution, along a constant *Q* scan using Reslib [29], to our data. Here $S(q,\omega)$ is treated using a Lorentzian approximation with the intensity scaled with $1/\omega$,

$$S(q,\omega) \propto \frac{1}{(1-e^{-\hbar\omega/k_BT})}\frac{1}{\omega}\frac{\Gamma}{(\hbar\omega-\hbar\omega_{ac}(q))^2+\Gamma^2} \qquad (3)$$

where Γ is the intrinsic HWHM of magnon spectra, characterizing the lifetime of the spin excitation, and the first term on the right hand side is the Bose factor. The resultant fitting spectra are shown by the solid curves in Fig. 3(a) and the contour map in the inset of Fig. 3(b) which captures the main features of the experimental data. The thus-obtained Γ values (inset of Fig. 4) are smaller than the instrumental energy resolution. This suggests that the observed broadening and intensity loss of the spectra mainly originate from the instrumental Q resolution contribution. We also fit an incoherent spectrum measured at $\boldsymbol{Q}$ = (0.1 0 3.5) using the Reslib program with a single mode approximation (SMA) to take into account the instrumental resolution. The fitting result matches well with the experimental data, indicating the accuracy of the Reslib fitting program. Besides, we also fit the magnetic excitation spectrum (data not shown) at (0 0 5) measured with E_f = 5.1 meV using a Be filter to have a better instrumental energy resolution ~ 0.70 meV and obtained a value of Γ ~ 0.17 meV that is close to the value shown in the inset of Fig. 4. Thus, these small yet finite values of Γ indicate a finite lifetime of the spin wave excitation. To further demonstrate this point, Figure 4 shows the comparison of two curves calculated using a Lorentzian approximation with different Γ values, Γ = 0.4 meV the fitted value and Γ = 0.1 meV as a smaller value for comparison, together with the curve obtained from the fitting using a SMA. Both Lorentzians of these widths and the SMA are convoluting with the full instrumental resolution and plotted with the experimental data measured at $\boldsymbol{Q}$ = (-0.2 0 5). Clearly Γ = 0.4 meV matches our data best. Therefore, the above discussions provide evidences of the necessity of including a finite linewidth in the model to describe the broadening of the spectra, implying a finite lifetime of the magnetic excitation that is presumably due to the existence of a non-negligible number of itinerant charge carriers even below T_{MI}. This is supported by various experimental observations: a) The in-plane resistivity of $Ca_3Ru_2O_7$ shows

metallic behavior at low temperatures, although the resistivity along the c-axis enhances only by one order of magnitude or so below T_{MI} [33]; b) ARPES experiments reveal a small Fermi surface pocket surviving at low temperatures [34]; c) Optical conductivity measurements show the existence of pseudogap opening below T_{MI} which argue that the in-plane metallic behavior is triggered by hopping of the carriers due to the strong hybridization between different Ru t_{2g} orbital states [35]. Thus, it is reasonable to attribute the finite lifetime of the spin wave excitation observed in our experiment to the existence of itinerant charge carriers within the planes which induces the magnon broadening *via* the magnon-itinerant charge carrier scattering, a feature similar to the ferromagnetic metallic bilayer manganite [27].

In conclusion, spin wave excitations of the bilayer ruthenate $Ca_3Ru_2O_7$ has been probed by inelastic neutron scattering measurements and are well described by a Heisenberg model with nearest-neighbor interactions. The system shows a spin gap of 7 meV and the intrabilayer exchange interaction along the c-axis is found to be much larger than the in-plane intralayer interaction. The finite lifetime of the magnetic excitation is presumably associated with a small number of itinerant charge carriers within the planes.

Experimental work at ORNL was supported by the Scientific User Facilities Division, Office of Basic Energy Sciences, DOE, and the work at Tulane is supported by the DOD ARO under Grant No. W911NF0910530 and the NSF under grant DMR-0645305. X. K. gratefully acknowledges helpful discussions with Dr. David Singh and the financial support by the Clifford G. Shull Fellowship at ORNL.

FIGURE CAPTIONS

Figure 1. Schematics of the crystal structure, spin structure, and magnetic interactions (interlayer interaction $J_{//}$ and intrabilayer interaction $J_{\perp}$) of $Ca_3Ru_2O_7$. Blue balls are Ca atoms, Grey octahedra are RuO_6 octahedra, and Red arrows represent Ru spins which are ferromagnetically aligned within the bilayer while antiferromagnetically aligned between bilayers.

Figure 2. (a) Constant-Q scan showing the dispersionless feature along L, evidence of a very weak interbilayer interaction; (b) L-dependence of neutron scattering intensity with E = 7 meV at T = 10 K and 80 K. Solids curves are the fits described in the text.

Figure 3. (a) Constant-Q scans with various values of H. Solid curves are the fits by convoluting with the full instrumental resolution. (b) E-(H 0 5) contour map with $\Delta H = 0.05$ measured at T = 10 K. Cycle symbols are the magnon peak values extracted from data fittings with a simple Gaussian function and the pink solid curve is the fitted magnetic dispersion curve. Inset shows the calculated contour map by taking into account the instrumental resolution described in the text.

Figure 4. Comparison of fitting results using the Reslib program with a single mode approximation(SMA) (purple curve) and using the Reslib program but with a Lorentzian function with two different Γ values, Γ = 0.1 (blue curve) and 0.4 meV (red curve), with the experimental data measured at $\boldsymbol{Q}$ = (-0.2 0 5). χ^2 values of these three fittings are 6.60, 3.36, and 1.21 respectively, indicating the necessity of including a finite linewidth 2Γ to describe the spectra. Inset shows the fitted 2Γ values described in the text.

[1] A. P. Mackenzie and Y. Maeno, Rev. Mod. Phys. **75**, 657 (2003).

[2] Y. Maeno, H. Hashimoto, K. Yoshida, S. Nishizaki, T. Fujita, J. Bednorz, and F. Lichtenberg, Nature **372**, 534 (1994).

[3] A. Callagham, C. W. Moeller, and R. Ward, Inorg. Chem. **5**, 1572 (1966).

[4] S. I. Ikeda, Y. Maeno, S. Nakatsuji, M. Kosaka, and Y. Uwatoko, Phys. Rev. B **62**, R6089 (2000).

[5] S. A. Grigera, R. S. Perry, A. J. Schofield, M. Chiao, S. R. Julian, G. G. Lonzarich, S. I. Ikeda, Y. Maeno, A. J. Millis, and A. P. Mackenzie, Science **294**, 329 (2001).

[6] R. A. Borzi, S. A. Grigera, J. Farrell, R. S. Perry, S. J. S. Lister, S. L. Lee, D. A. Tennant, Y. Maeno, and A. P. Mackenzie, Science **315**, 214 (2007).

[7] Y. Sidis, M. Braden, P. Bourges, B. Hennion, S. NishiZaki, Y. Maeno, and Y. Mori, Phys. Rev. Lett. **83**, 3320 (1999).

[8] F. Servant, B. Fåk, S. Raymond, J. P. Brison, P. Lejay, and J. Flouquet, Phys. Rev. B **65**, 184511 (2002).

[9] M. Braden, Y. Sidies, P. Bourges, P. Pfeuty, J. Kulda, Z. Mao, and Y. Maeno, Phys. Rev. B **66**, 064522 (2002).

[10] L. Capogna, E. M. Forgan, S. M. Hayden, A. Wildes, J. A. Duffy, A. P. Mackenzie, R. S. Perry, S. Ikeda, Y. Maeno, and S. P. Brown, Phys. Rev. B **67**, 012504 (2003).

[11] M. B. Stone, M. D. Lumsden, R. Jin, B. C. Sales, D. Mandrus, S. E. Nagler, and Y. Qiu, Phys. Rev. B **73**, 174426 (2006).

[12] S. Nakatsuji and Y. Maeno, Phys. Rev. Lett. **84**, 2666 (2000).

[13] O. Freidt, M. Braden, G. André, P. Adelmann, S. Nakatsuji, and Y. Maeno, Phys. Rev. B **63**, 174432 (2001).

[14] O. Freidt, P. Steffens, M. Braden, Y. Sidis, S. Nakatsuji, and Y. Maeno, Phys. Rev. Lett. **93**, 147404 (2004).

[15] G. Cao, S. C. McCall, J. E. Crow, and R. P. Guertin, Phys. Rev. B **56**, 5387 (1997).

[16] S. Ikeda, Y. Maeno, and T. Fujita, Phys. Rev. B **57**, 978 (1998).

[17] Z. Qu, L. Spinu, H. Yuan, V. Dobrosavljevic, W. Bao, J. W. Lynn, M. Nicklas, J. Peng, T. Liu, D. Fobes, E. Flesch, and Z. Q. Mao, Phys. Rev. B **78**, 180407(R) (2008).

[18] J. Peng, Z. Qu, B. Qian, D. Fobes, T. Liu, X. Wu, H. M. Pham, L. Spinu, and Z. Q. Mao, Phys. Rev. B **82**, 024417 (2010).

[19] Cao, S. McCall, J. E. Ceow, and R. P. Guertin, Phys. Rev. Lett. **78**, 1751 (1997).

[20] J. F. Karpus, R. Gupta, H. Barath, and S. L. Cooper, Phys. Rev. Lett. **93**, 167205 (2004).

[21] Y. Yoshida, S. I. Ikeda, H. Matsuhata, N. Shirakawa, C. H. Lee, and S. Katano, Phys. Rev. B **72**, 054412 (2005).

[22] W. Bao, Z. Q. Mao, Z. Qu, and J. W. Lynn, Phys. Rev. Lett. **100**, 247203 (2008).

[23] G. Cao, L. Balicas, Y. Xin, E. Dagotto, J. E. Crow, C. S. Nelson, and D. F. Agterberg, Phys. Rev. B. **67**, 060406(R) (2003).

[24] D. J. Singh and S. Auluck, Phys. Rev. Lett. **96**, 097203 (2006).

[25] J. F. Karpus, C. S. Snow, R. Gupta, H. Barath, S. L. Cooper, and G. Cao, Phys. Rev. B **73**, 134407 (2006).

[26] T. Chatterji, L. P. Regnault, P. Thalmeier, R. Suryanarayanan, G. Dhalenne, and A. Revcolevschi, Phys. Rev. B **60**, R6965 (1999).

[27] T. G. Perring, D. T. Adroja, G. Chboussant, G. Aeppli, T. Kimura, and Y. Tokura, Phys. Rev. Lett. **87**, 217201 (2001).

[28] K. Hirota, S. Ishihara, H. Fujioka, M. Kubota, H. Yoshizawa, Y. Moritomo, Y. Endoh, and S. Maekawa, Phys. Rev. B **65**, 064414 (2006).

[29] http://www.neutron.phys.ethz.ch/personal/reslib/index.html

[30] T. Chatterji, L. P. Regnault, P. Thalmeier, R. van de Kamp, W. Schmidt, A. Hiess, P. Vorderwisch, R. Suryanarayanan, G. Dhalenne, and A. Revcolevschi, J. Alloys and Compounds **326**, 15 (2001).

[31] L. Vasiliu-Doloc, J. W. Lynn, A. H. Moudden, A. M. de Leon-Guevara, and A. Revcolevschi, Phys. Rev. B **58**, 14913 (1998).

[32] P. Dai, H. Y. Hwang, J. Zhang, J. A. Fernandez-Baca, S.-W. Cheong, C.Kloc, Y. Tomioka, and Y. Tokura, Phys. Rev. B **61**, 9553 (2000).

[33] Y. Yoshida, I. Nagai, S.I. Ikeda, N. Shirakawa, M. Kosaka, and N. Mori, Phys. Rev. B **69**, 220411 (2004).

[34] F. Baumberger, N. J. c. Ingle, N. Kikugawa, M. A. Hossain, W. Meevasana, R. S. Perry, K. M. Shen, D. H. Lu, A. Damascelli, A. Rost, A. P. Mackenzie, Z. Hussain, and Z. X. Shen, Phys. Rev. Lett. **96**, 107601 (2006).

[35] J. S. Lee, S. J. Moon, B. J. Yang, J. Yu, U. Schade, Y. Yoshida, S. I. Ikeda, and T. W. Noh, Phys. Rev. Lett. **98**, 097403 (2007).

Figure 1.

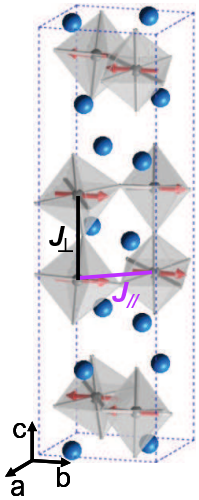

Figure 1 LC12959B 24JUN2011

Figure 2.

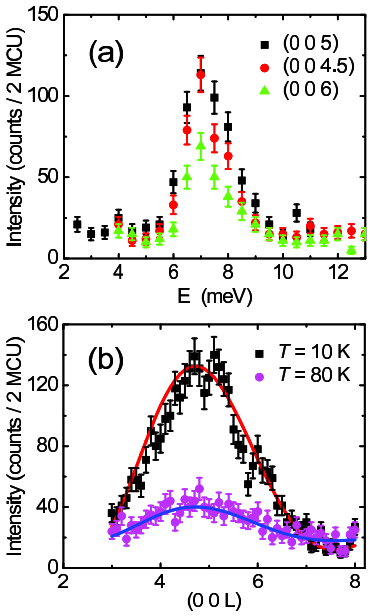

Figure 2 LC12959B 24JUN2011

Figure 3.

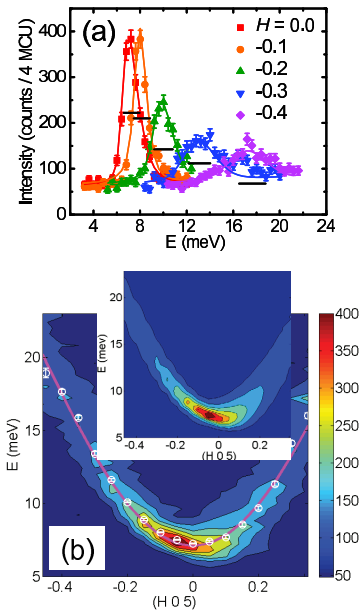

Figure 3 LC12959B 24JUN2011

Figure 4.

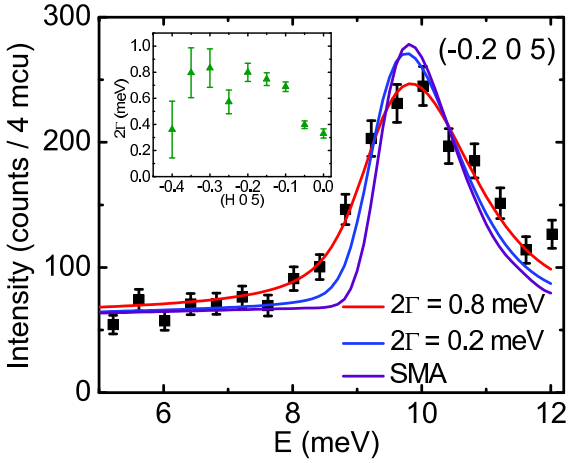

Figure 4 LC12959B 24JUN2011